Navarrete Algaba, L.; Balaguer Ramirez, M.; Vert Belenguer, VB.; Serra Alfaro, JM. (2016). Optimization of SOFC Composite Cathodes Based on LSM and Doped Cerias Ce0.8Ln0.2O2 (Ln = Gd, Er, Tb and Pr). Journal of The Electrochemical Society. 163(13):1440-1443. doi:10.1149/2.1081613jes.

J. Electrochem. Soc. ***2016 volume 163, issue 13, F1440-F1443***

doi: 10.1149/2.1081613jes

Optimization of SOFC composite cathodes based on LSM and doped cerias $Ce_{0.8}Ln_{0.2}O_{2-\delta}$ (Ln=Gd, Er, Tb and Pr)

Laura Navarrete, María Balaguer, Vicente B. Vert, José M. Serra*

Instituto de Tecnología Química (Universitat Politècnica de València – Consejo Superior de Investigaciones Científicas), Av. Los Naranjos, s/n, 46022 Valencia (SPAIN)

* corresponding author: jmserra@itq.upv.es; Phone: +34.963879448

Keywords: fuel cells; cobalt; composite; cathode; ceria; electrochemical impedance spectroscopy

Abstract

Composites made of $La_{1-x}Sr_xMnO_{3-\delta}$ (LSM) and lanthanide doped ceria ($Ce_{0.8}Ln_{0.2}O_{2-\delta}$, Ln=Gd, Er, Tb and Pr) have been proposed as robust and high-performing solid oxide fuel cell cathodes. The addition of small amounts of highly-dispersed CoO_x into the electrode promoted the formation of bridges among LSM-ceria particles. These resulted in the reduction of the required sintering temperature due to the enhancement of the sintering and proper ionic and electronic percolation pathways. In addition, Pr as a multivalent cation dopant in ceria showed the best electrochemical results towards oxygen reduction when the electrode sintering temperature is kept at 1000 °C.

1. Introduction

Lanthanum strontium manganite, $La_{1-x}Sr_xMnO_{3-\delta}$ (LSM) is one of the cathode materials most commonly employed for solid oxide fuel cells (SOFC). LSM combines high electronic conductivity with remarkable catalytic properties and high thermal and mechanical stability. In addition, LSM is compatible with most electrolyte materials such as yttria stabilized zirconia [1-3], doped ceria, and several perovskites [4]. However, at low temperatures, the lack of ionic conductivity limits the application of LSM as a SOFC cathode. Therefore, composites made of $La_{1-x}Sr_xMnO_{3-\delta}$ (LSM) and lanthanide doped zirconia or ceria ($Ce_{1-y}Ln_yO_{2-\delta}$) have been proposed as SOFC cathodes[5, 6]. The addition of the ceria phase enhances the ionic transport, increasing the triple phase boundary (TPB) length in the electrode where gaseous oxygen comes into contact with the ion and electron conducting phases, and the electrochemical reactions take place [7]. Furthermore, by introducing lanthanide elements with mixed valence (as Pr and Tb) in the ceria lattice, mixed ionic-electronic conductivity (MIEC) may be promoted even at high oxygen partial pressures ($pO_2 > 10^{-5}$ atm) [8-11]. Thus, the TPB area is further increased since the whole surface area of the ceria in contact with the gas is active for the electrochemical reaction in addition to the LSM-electrolyte interface.

CoO_x, has been reported as a ceria sintering aid and promoter of the electronic conductivity through the grain boundaries [12-15]. Here, the addition of CoOx is intended to promote the formation of an electronic network that bridges the transport of electrons with the LSM particles. A study of this effect on the performance of a SOFC cathode has been made by impregnating CoO_x in an optimum amount of 2 mol% [13] to $Ce_{0.8}Gd_{0.2}O_{1.9}$ and $Ce_{0.8}Pr_{0.2}O_{2-\delta}$, being the most widely studied composition and the best electrode tested, respectively.

2. Experimental

Different $Ce_{0.8}Ln_{0.2}O_{2-\delta}$ (Ln = Pr, Gd, Tb and Er) compositions have been synthesized by co-precipitation method, as described in reference [16]. $La_{0.8}Sr_{0.2}MnO_3$ (LSM) powder was purchased from

Fuel Cell Materials (USA). Powder X-ray diffraction (XRD) was used for the identification of the crystalline phases by a PANalytical Cubix fast diffractometer that uses CuKα1 radiation (λ = 1.5406 Å) and a X′Celerator detector in Bragg−Brentano geometry. XRD patterns were analyzed by X'Pert Highscore Plus software.

Electrical conductivity measurements of the ceria-based compounds ($Ce_{0.8}Ln_{0.2}O_{2-\delta}$) were conducted by standard four-point DC technique on rectangular bars sintered at 1300 ºC for 5 h (achieving >98% density). The measurements were carried out in air and the current was supplied by a Keithley 2601 programmable current source and voltage drop through the sample was detected by a Keithley 3706 multimeter.

Screen-printable inks made of composite cathodes were prepared by mixing LSM and ceria-based powders with a 6% wt. ethylcellulose - terpineol solution in a three roll milling (1:1:2 weight ratio). The ratio between both phases is 50/50 % w/w and was selected taking into account a previous study of different LSM/ $Ce_{0.8}Gd_{0.2}O_{2-\delta}$ ratios[17]. These inks were applied on both sides of a fully-dense $Ce_{0.8}Gd_{0.2}O_{2-\delta}$ (2% wt. Co) ~1 mm-thick electrolytes, provided by IKTS Fraunhofer (Germany). Porous electrodes were obtained after calcination at 1150 ºC for 2 h. Further electrode optimization was carried out for LSM/$Ce_{0.8}Gd_{0.2}O_{2-\delta}$ and LSM/$Ce_{0.8}Pr_{0.2}O_{2-\delta}$, using 2 mol % Co as sintering aid, and sintering the electrodes at 1000 ºC and 1150 ºC. Finally a top screen-printed gold mesh was further applied on the electrodes in order to warrant proper current collection. Particle size and morphology of the powder samples as well as electrode microstructure was analyzed by SEM imaging in a JEOL 6360 microscope.

As-fabricated symmetrical cells were tested by means of electrochemical impedance spectroscopy (EIS) measurements using a 0 V DC - 20 mV AC amplitude signal using a Solartron 1470E/1455 FRA device. Samples were tested in air in the 700-900 ºC range.

3. Results and discussion

3.1. LSM and ceria-based composites characterization

XRD analysis of $Ce_{0.8}Gd_{0.2}O_{2-\delta}$ (CG82), $Ce_{0.8}Pr_{0.2}O_{2-\delta}$ (CP82), $Ce_{0.8}Er_{0.2}O_{2-\delta}$ (CE82) and $Ce_{0.8}Tb_{0.2}O_{2-\delta}$ (CT82) powders confirms the formation of the fluorite phase [18, 19]. The compatibility of the different LSM/ceria composites was checked by XRD after calcining a 1:1 mixture of powders at 1150 ºC (2h). The XRD patterns of the sintered composites (Figure 1) demonstrate the compatibility, since all peaks belong to the fluorite and LSM perovskite phases, and no additional peaks are observed.

The transport properties of the $Ce_{0.8}Ln_{0.2}O_{2-\delta}$ series were evaluated by measuring the total conductivity in air as a function of the temperature (Fig. 2a). The highest conductivity value is obtained for CG82 at high temperatures, however at low temperatures CP82 has higher conductivity than CG82 improving the total conductivity. Electronic levels are introduced in the bandgap when Pr is incorporated in the structure [10], the electronic conductivity is enhanced via small polaron hopping between Pr^{3+} and Pr^{4+}. Around 700 ºC the concentration of both oxidation states is equal producing a maximum in the small polaron hopping. The reduction in the conductivity of CE82 can be attributed to small impurities of Er_2O_3, which increases the resistivity of ceria [20]. XRD analysis of CE82 samples revealed the presence of Er_2O_3 impurities with main diffraction peaks appearing at 31º and 62º. Finally, CT82 exhibits similar behavior than CP82 due to the mixed valence of Tb, but in this case the recorded total conductivity is the lowest one.

The electrochemical behavior of the four LSM-based composite cathodes was studied by EIS using symmetrical cells. The polarization resistance (Rp) recorded in air is plotted as function of temperature (Figure 2b). The electrochemical performance is notably improved by the introduction of the ionic phase in the electrode. Composite cathodes show Rp values one order of magnitude lower for the whole range of operation temperature when compared with the pure LSM cathode. This effect is due to the TPB enlargement along the whole electrode. The oxygen reduction reaction is not restricted to the

LSM-electrolyte interface, but extended to a much larger active area when ceria is incorporated in the electrode. In addition, electrodes with cerias comprising a cation with mixed valence (Pr, Tb) exhibit the lowest polarization resistance values, being the CP82 the best electrode tested. The same trend as in the conductivity measurements is obtained between CP82 and CT82, CP82 being the compound with the highest conductivity and the lowest Rp. In these two electrode compositions, the promotion of electronic conduction in the ceria phase enables to enlarge the TPB while the ionic conductivity is preserved. Despite the lower conductivity, CE82 exhibits an improvement of the widely studied CG82 compound.

The activation energy (E_a) is reduced from 1.83 eV for LSM to 1.46 eV for LSM/CT82 and LSM/CE82, 1.36 eV for LSM/CG82 and 1.25 eV for LSM/CP82, the lowest E_a obtained within this set of samples. The good performance of the LSM/CP82 electrode could be associated with the higher conductivity due to the high population of mobile oxygen and electronic defects combined with electron hopping, and the catalytic activity reported for PrO_x as O_2 reduction catalyst [21, 22].

3.2. CoOx incorporation in the composite electrodes

Further improvement of the cell was performed by impregnating the reference electrode material (LSM/CG82) and the best performance electrode material (LSM/CP82) with 2 mol% CoO_x, prior to electrode coating and firing. Note that no secondary phases were detected in the electrodes incorporating CoO_x and Co atoms appear evenly distributed over the fluorite phase, as revealed by EDX analysis of tested electrodes. Figure 2c shows the polarization resistance of the LSM/CG82 and LSM/CP82 with and without CoO composite cathodes sintered at 1150 °C (to compare with reference cathodes) [23] and at 1000 °C. The addition of CoO_x to the ceria phase was detrimental when high calcination temperature was used, i.e. 1150 °C, both for LSM/CP82 and LSM/CG82. The polarization resistance increases with respect to the composite without CoO_x. This effect originates from (i) the larger particles of the electrodes containing CoO_x (due to the sintering promotion in cerias) that causes a loss in surface area; and (ii) the agglomeration of CoO_x in the grain boundaries. This is detrimental to the electrical conductivity and

previous works reported that a maximum in conductivity appears when the calcination temperature is 1000 °C [24]. Therefore, new CoO_x-containing electrodes were sintered at 1000 °C aiming to (i) obtain a comparable particle size with respect to the pristine electrode (CoO_x free), and (ii) keep the CoO_x spread on the ceria grain boundaries [24]. As observed in Figure 2c, the polarization resistance of these electrodes decreases, especially in the high temperature region in case of LSM/CP82Co treated at 1000 °C (inset of Figure 2c). To complete the electrode series, CoO_x-free electrodes were prepared and calcined at 1000 °C but the sintering extent was not enough and the electrodes detached from the electrolyte [25]. As a consequence, the electrode testing by EIS was precluded.

SEM images analysis (Figure 3) reveals important differences between particle size distribution of LSM/CP82 1150 °C and LSM/CP82Co 1150 °C. Therefore, the observed increase in Rp is in accordance to such grain growth and the associated decrease in surface area. The smaller difference observed among LSM/CG82 1150 °C and LSM/CG82Co 1150 °C, is also corresponding to a more similar Rp values. The smallest particle sizes observed for the electrodes sintered at 1000 °C show the lowest Rp due to the large surface area available for the oxygen reduction reaction (ORR).

In order to discern the different processes involved in the electrode operation, the electrochemical impedance spectra are showed in Figure 4 for all six tested cathodes measured in air. The electrolyte and contact resistances were subtracted in the figure for direct comparison. It can be inferred that Rp diminished with decreasing particle size and, thus, the highest performance is reached by CoO_x-containing electrodes calcined at 1000 ºC. The conduction mechanisms ascertained in the monovalent (Gd) or bivalent (Pr) doped ceria lead to the different limitations observed in the cathodes that would be explained below in detail, apart from the particle size. Although the ionic conductivity of the CG82 is higher than that for CP82, oxygen surface exchange coefficient for both doped cerias (without CoO_x) is similar due to the excellent oxygen exchange activity of CP82 [26]. Consequently, the difference in the behavior for both composites cannot be attributed to the surface oxygen exchange rate.

When Pr is used as dopant, the double valence confers mixed ionic and electronic conductivity to the ceria and this stems from the formation of a praseodymium impurity band within the CeO_2 band gap [10]. Hence, the electronic conduction provided by the LSM is not blocked and holes can diffuse through the grain boundaries of the neighboring ceria grain, which is observed by the lack of processes at medium frequencies (MF). Medium and high frequencies (HF) processes are only ascertained when the surface area is high enough not to limit the transport, which occurs when sintering at low temperature and with CoO_x. Figure 3b shows that LSM/CP82 and LSM/CP82Co cathode at 1150 ºC are limited in the low frequency (LF, 0.1-100 Hz), which correspond to surface processes [27]. The highest resistance observed for LSM/CP82Co at 1150 ºC is in agreement with the biggest particle size and subsequent less surface area. Contrarily, for the LSM/CP82Co at 1000 ºC, the LF contribution disappears and new arcs at medium (MF, 10-1000 Hz) and high frequencies (HF, 1-100 kHz) are observed. The MF arc is typically associated to surface transport of oxygen ion or intermediate species through the interface between LSM and doped ceria, while the contribution at HF is related to the transport of oxygen from the electrode to the electrolyte and the charge transfer [27].

On the other hand, the operation of LSM/CG82 (with and without CoO_x) electrode calcined at 1150 °C are limited by processes occurring at MF to HF, while LSM/CG82 at 1000 °C shows a broad HF contribution. LSM/CGO82 has two contributions coupled at HF. For composites, it can be related with the transport of oxygen intermediates or oxide ions between the interface of CGO and LSM and through the CGO of the composite. Sunde et al. suggested that if there are some isolated phases, lacking the percolation, the impendace may be affected and this effect appears at high frequencies [28, 29]. Jogersen et al. [30] discussed the different contributions that usually appear in a composite impedance spectrum. They highlighted the presence of an arc at medium frequencies in the EIS spectra, always present in composite electrodes. The TPB length highly influences the magnitude of this arc, and sometimes this contribution becomes the limiting resistance in the electrode performance. Moreover, that limiting step has been situated as essential for the oxygen reduction reaction. The resistance obtained at this MF-HF frequency

for LSM/CG82 with and without CoO_x is related with this process, since the pure ionic conductivity of the CG820 could block the electronic transport of LSM. At low sintering temperatures (1000 ºC) the arc in LSM/CGO82Co is shifted to higher frequencies, although the HF arc decreases as a consequence of the CoO_x electronic contribution and good dispersion. In comparison with LSM/CPO82, whose resistance at higher frequencies is lower, the plot suggests that a mixed ionic electronic conductivity can improve the transport processes from the electrode to the electrolyte.

In summary, the cell performance is strongly affected by the electrode microstructure [31, 32]. Decreasing sintering temperatures enlarge the TPB since small grains are obtained, resulting in lower polarization resistance (Figure 3). The best sintering temperature is a tradeoff between a long TPB and good electrical and optimal physical contact among LSM and GDC grains [33]. In Table 1, Rp values achieved at 650ºC for LSM/CP82Co (1000 ºC) electrode are compared with values obtained using distinct state-of-the-art SOFC cathodes.

4. Conclusions

Different compatible materials with LSM were synthesized and mixed to form composite electrodes as SOFC cathodes. The electrode comprising $La_{0.8}Sr_{0.2}MnO_3$ / $Ce_{0.8}Pr_{0.2}O_{2-\delta}$ exhibited the lowest polarization resistance in the temperature range of 700 to 900 ºC. The reached polarization resistance values are one order of magnitude below the values reached for classic $La_{0.8}Sr_{0.2}MnO_3$ / YSZ electrodes. The nature of the dopant and the particle size influences the cathode performance. Higher surface area provides more reaction sites where the oxygen can be dissociated and reduced to O^{2-}, whereas a mixed ionic-electronic conductor provides additional pathways for the oxygen anions to reach the electrolyte surface as well as for the electrons to move along the whole cathode. These effects where achieved by introducing Pr in the ceria, a cation with two stable oxidation states under the applied operation conditions. On the other hand, the addition of CoO_x influences the cathode transport properties by introducing more electronic pathways, but when it is sintered at high temperature (1150 ºC), the

influence in the microstructure is more evident. Three effects are observed, i) the CoO_x promotes the particle size growing, being more detrimental as the sintering temperature increases, and ii) CoO_x allows the attachment of the electrode to the electrolyte when low sintering temperatures are intended, and iii) CoO_x may contribute to the electronic conductivity when it is properly spread in the grain boundaries. Therefore, the best cathode results were obtained for the composite made from LSM/CP82Co sintered at 1000 °C.

Acknowledgment

This work was supported by funding from Spanish Government (MINECO) (SEV-2012-0267 and ENE2014-57651 grants).

References

1. F. Liang, J. Chen, S. P. Jiang, B. Chi, J. Pu, and L. Jian, *Electrochemistry Communications,* **11** (5), 1048-1051 (2009).
2. K. S. Yun, C.-Y. Yoo, S.-G. Yoon, J. H. Yu, and J. H. Joo, *Journal of Membrane Science,* **486** 222-228 (2015).
3. L. Jia, K. Li, D. Yan, X. Wang, B. Chi, J. Pu, L. Jian, and S. Yuan, *Rsc Advances,* **5** (10), 7761-7765 (2015).
4. E. N. Armstrong, K. L. Duncan, D. J. Oh, J. F. Weaver, and E. D. Wachsman, *Journal of The Electrochemical Society,* **158** (5), B492-B499 (2011).
5. R. Kiebach, P. Zielke, J. V. T. Hogh, K. Thyden, H. J. Wang, R. Barford, and P. V. Hendriksen, *Fuel Cells,* **16** (1), 80-88 (2016).
6. L. Navarrete, C. Solis, and J. M. Serra, *Journal of Materials Chemistry A,* **3** (32), 16440-16444 (2015).
7. J. Nielsen and J. Hjelm, *Electrochimica Acta,* **115** (0), 31-45 (2014).
8. M. Balaguer, C. Solís, and J. M. Serra, *Chemistry of Materials,* **23** (9), 2333-2343 (2011).
9. M. Balaguer, C.-Y. Yoo, H. J. Bouwmeester, and J. M. Serra, *Journal of Materials Chemistry A,* **1** (35), 10234-10242 (2013).
10. H. L. Tuller, S. R. Bishop, D. Chen, Y. Kuru, J. J. Kim, and T. S. Stefanik, *Solid State Ionics,* **225** 194-197 (2012).
11. D. P. Fagg, D. Pérez-Coll, P. Núñez, J. R. Frade, A. L. Shaula, A. A. Yaremchenko, and V. V. Kharton, *Solid State Ionics,* **180** (11–13), 896-899 (2009).
12. M. Balaguer, C. Solís, and J. M. Serra, *The Journal of Physical Chemistry C,* **116** (14), 7975-7982 (2012).
13. D. P. Fagg, J. C. C. Abrantes, D. Pérez-Coll, P. Núñez, V. V. Kharton, and J. R. Frade, *Electrochimica Acta,* **48** (8), 1023-1029 (2003).
14. D. P. Fagg, A. L. Shaula, V. V. Kharton, and J. R. Frade, *Journal of Membrane Science,* **299** (1–2), 1-7 (2007).
15. K. Schmale, M. Grünebaum, M. Janssen, S. Baumann, F. Schulze-Küppers, and H.-D. Wiemhöfer, *physica status solidi (b),* **248** (2), 314-322 (2011).
16. M. Balaguer, C. Solis, and J. M. Serra, *J. Phys. Chem. C,* **116** (14), 7975-7982 (2012).
17. E. P. Murray and S. A. Barnett, *Solid State Ion.,* **143** (3-4), 265-273 (2001).
18. T. Mori, Y. Wang, J. Drennan, G. Auchterlonie, J.-G. Li, and T. Ikegami, *Solid State Ionics,* **175** (1–4), 641-649 (2004).
19. K. C. Anjaneya, G. P. Nayaka, J. Manjanna, G. Govindaraj, and K. N. Ganesha, *Journal of Alloys and Compounds,* **578** 53-59 (2013).
20. S. Kuharuangrong, *Journal of Power Sources,* **171** (2), 506-510 (2007).
21. J. M. Serra and V. B. Vert, *ChemSusChem,* **2** (10), 957-961 (2009).
22. J. M. Serra and V. B. Vert, *Journal of The Electrochemical Society,* **157** (10), B1349-B1357 (2010).
23. M. Balaguer, V. B. Vert, L. Navarrete, and J. M. Serra, *Journal of Power Sources,* **223** (0), 214-220 (2013).
24. C. Solís, M. Balaguer, F. Bozza, N. Bonanos, and J. M. Serra, *Applied Catalysis B: Environmental,* **147** 203-207 (2014).
25. B. Ahmed, S.-B. Lee, R.-H. Song, J.-W. Lee, T.-H. Lim, and S.-J. Park, *J Solid State Electrochem,* **18** (2), 435-443 (2014).
26. C.-Y. Yoo. Universiteit Twente, Enschede, 2012.
27. S. B. Adler, *Chem. Rev.,* **104** (10), 4791-4843 (2004).
28. S. Sunde, *Electrochimica Acta,* **42** (17), 2637-2648 (1997).

29. S. Sunde, *Journal of the Electrochemical Society,* **143** (6), 1930-1939 (1996).
30. M. J. Jorgensen and M. Mogensen, *J. Electrochem. Soc.,* **148** (5), A433-A442 (2001).
31. L. Baqué, A. Caneiro, M. S. Moreno, and A. Serquis, *Electrochemistry Communications,* **10** (12), 1905-1908 (2008).
32. K. Chen, N. Ai, C. Lievens, J. Love, and S. P. Jiang, *Electrochemistry Communications,* **23** 129-132 (2012).
33. M. J. Jorgensen, S. Primdahl, C. Bagger, and M. Mogensen, *Solid State Ionics,* **139** (1-2), 1-11 (2001).
34. G. Chen, J. Sunarso, Y. Wang, C. Ge, J. Yang, and F. Liang, *Ceramics International,* **42** (11), 12894-12900 (2016).
35. G. Chen, Y. Wang, J. Sunarso, F. Liang, and H. Wang, *Energy,* **95** 137-143 (2016).
36. W. G. Wang and M. Mogensen, *Solid State Ion.,* **176** (5–6), 457-462 (2005).
37. W. Zhou, Z. Shao, R. Ran, P. Zeng, H. Gu, W. Jin, and N. Xu, *Journal of Power Sources,* **168** (2), 330-337 (2007).

Figures caption:

Figure 1: XRD patterns of the composite compatibility test at 1150 ºC during 2 hours in air.

Figure 2: Electrochemical characterization (a) total conductivity measurements in air of the different fluorites and (b) polarization resistance obtained for composite electrodes in air. E_a values included in the legend (electrodes sintered at 1150 ºC) (c) polarization resistance of the six different composite cathodes sintered at different temperatures and with or without Co.

Figure 3. SEM micrographs of the composite electrodes tested; (a) LSM/CG82 1150 ºC, (b) LSM/CG82Co 1150 ºC, (c) LSM/CG82Co 1000 ºC, (d) LSM/CP82 1150 ºC, (e) LSM/CP82Co 1150 ºC and (f) LSM/CP82Co 1000 ºC.

Figure 4. Electrochemical impedance spectroscopy spectra recorded at 750 ºC in air (a) Nyquist and (b) Bode plots for the different LSM/CPO82 electrodes (c) Nyquist and (b) Bode plots LSM/CGO82 electrodes.

Figure 1

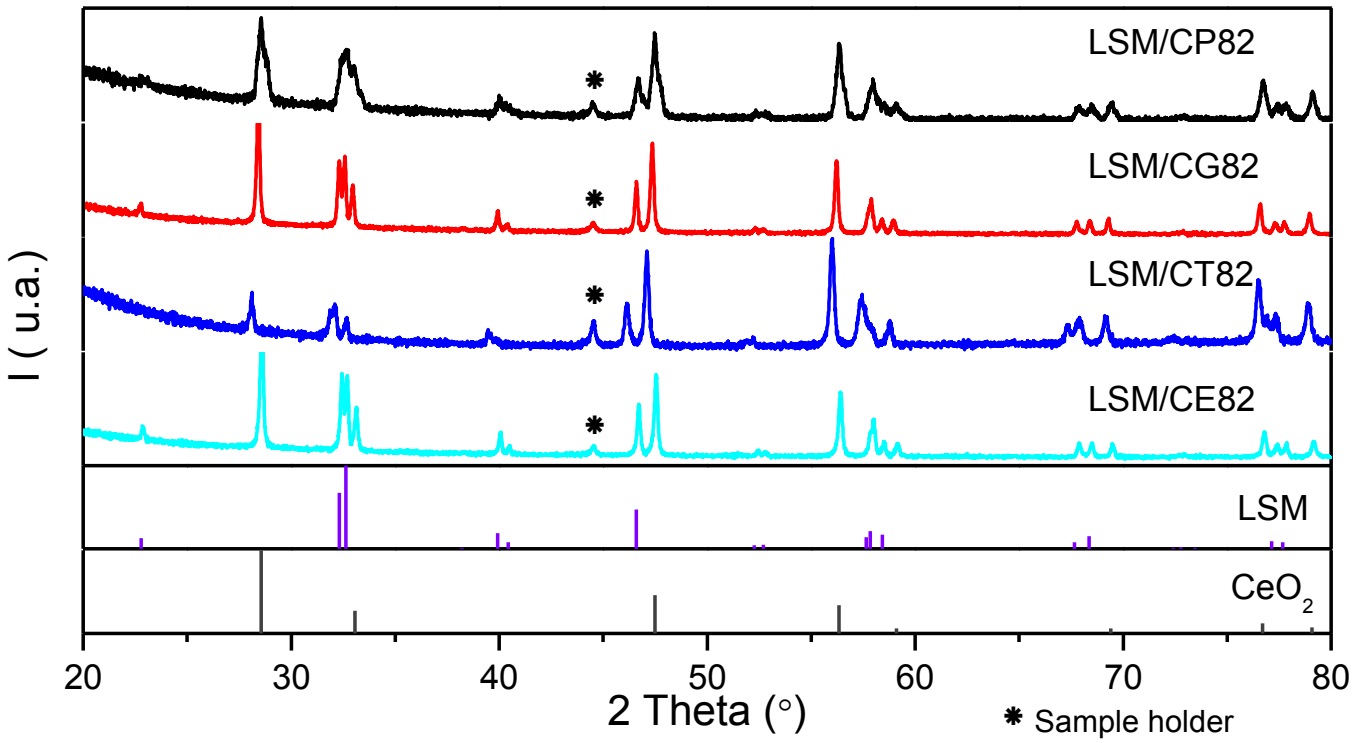
LSM/CP82
LSM/CG82
LSM/CT82
LSM/CE82
LSM
CeO2
I (u.a.)
20
30
40
50
60
70
80
2 Theta (°)
* Sample holder

Figure 2

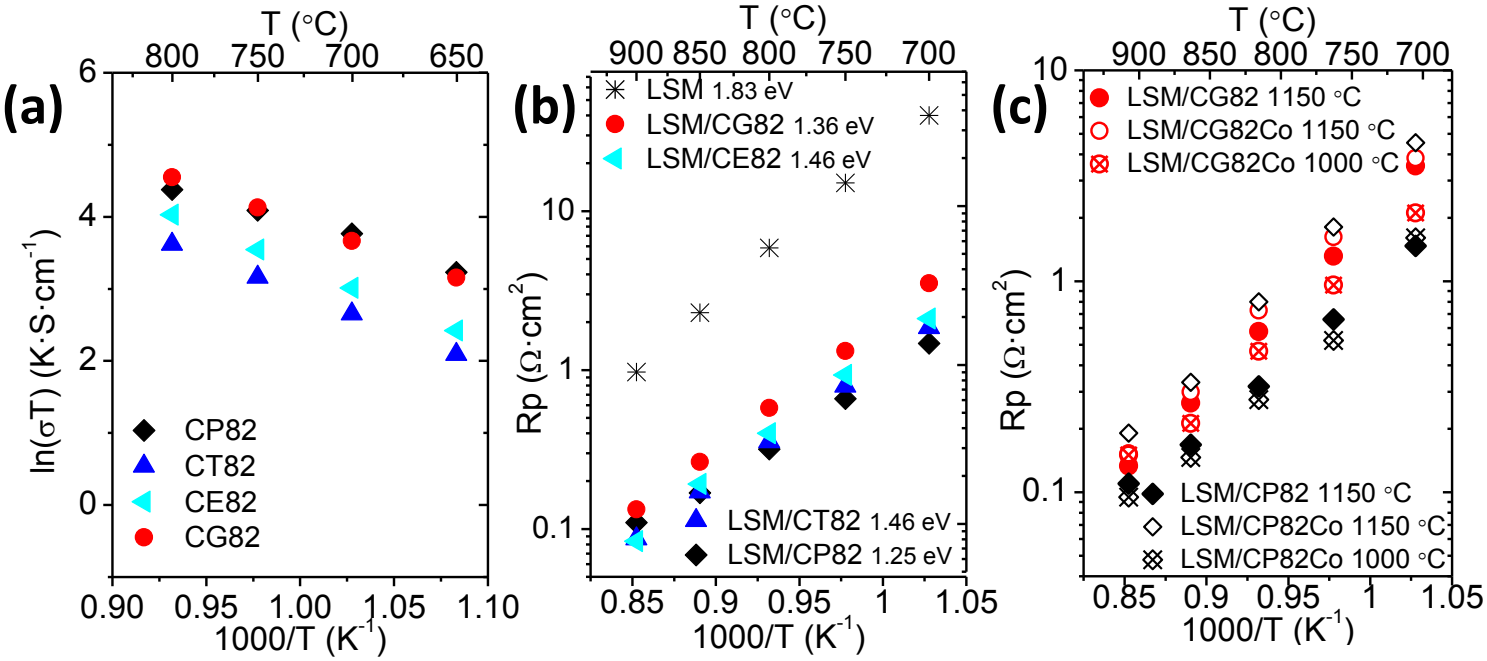
(a)
T (°C)
800 750 700 650
ln(σT) (K·S·cm-1)
CP82
CT82
CE82
CG82
1000/T (K-1)
(b)
T (°C)
900 850 800 750 700
Rp (Ω·cm2)
LSM 1.83 eV
LSM/CG82 1.36 eV
LSM/CE82 1.46 eV
LSM/CT82 1.46 eV
LSM/CP82 1.25 eV
1000/T (K-1)
(c)
T (°C)
900 850 800 750 700
Rp (Ω·cm2)
LSM/CG82 1150 °C
LSM/CG82Co 1150 °C
LSM/CG82Co 1000 °C
LSM/CP82 1150 °C
LSM/CP82Co 1150 °C
LSM/CP82Co 1000 °C
1000/T (K-1)

Figure 3

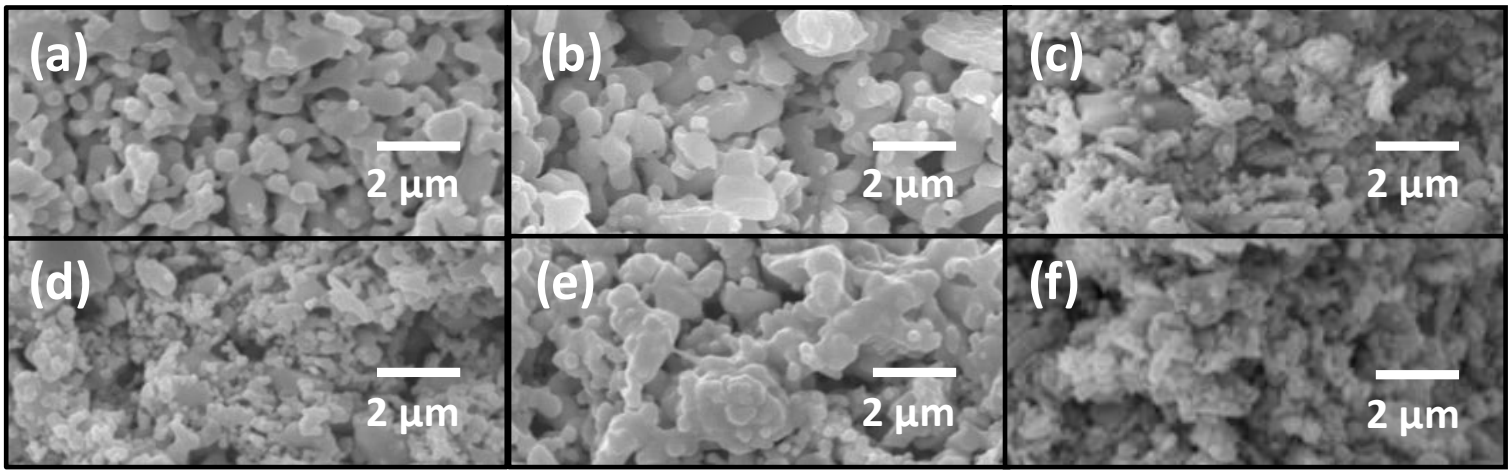

Figure 4

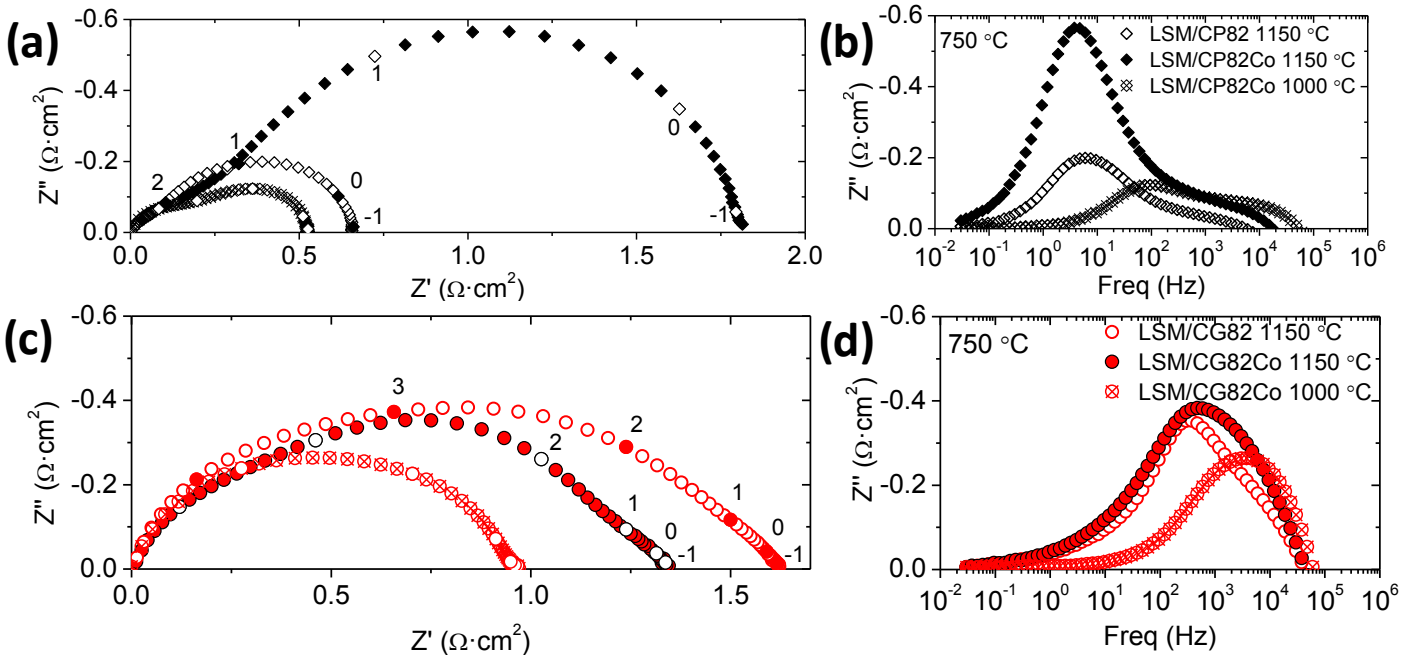
(a)
(b)
(c)
(d)
Z'' (Ω·cm²)
Z' (Ω·cm²)
Freq (Hz)
750 °C
LSM/CP82 1150 °C
LSM/CP82Co 1150 °C
LSM/CP82Co 1000 °C
LSM/CG82 1150 °C
LSM/CG82Co 1150 °C
LSM/CG82Co 1000 °C

Electrode Material	Rp ($\Omega \cdot cm^2$)	References
$Sr_{0.9}Sc_{0.175}Nb_{0.025}Co_{0.8}O_{3-\delta}$	≈0.04	[34]
$SrSc_{0.175}Nb_{0.025}Fe_{0.8}O_{3-\delta}$	≈0.09	[35]
$La_{0.8}Sr_{0.2}MnO_3$	≈22	[17]
$La_{0.8}Sr_{0.2}MnO_3$:YSZ (ZrO_2 Y_2O_3) (50:50)	≈16	[23]
$(La_{0.6}Sr_{0.4})_{1-x}Co_{0.2}Fe_{0.8}O_{3-\delta}$:$Ce_{0.9}Gd_{0.1}O_{3-\delta}$ (50:50)	≈0.27	[36]
$(La_{0.6}Sr_{0.4})_{1-x}Co_{0.2}Fe_{0.8}O_{3-\delta}$:$Ce_{0.9}Gd_{0.1}O_{3-\delta}$ (70:30)	≈0.31	[36]
$Ba_{0.5}Sr_{0.5}Co_{0.8}Fe_{0.2}O_{3-\delta}$ + $LaCoO_3$ (50:50)	≈0.17	[37]
$Ba_{0.5}Sr_{0.5}Co_{0.8}Fe_{0.2}O_{3-\delta}$ + $LaCoO_3$ (70:30)	≈0.09	[37]
$LaCoO_3$	≈39	[37]
$Ba_{0.5}Sr_{0.5}Co_{0.8}Fe_{0.2}O_{3-\delta}$	≈0.04	[37]
LSM/CP82 Co 1000ºC	≈3.5	Present study

Table 1: Polarization resistance at 650 ºC of representative state-of-the-art SOFC cathodes